Journal of Photochemistry & Photobiology, A: Chemistry 445 (2023) 115033

Contents lists available at ScienceDirect

Journal of Photochemistry & Photobiology, A: Chemistry

journal homepage: www.elsevier.com/locate/jphotochem

Development of fluorochromic polymer doped materials as platforms for temperature sensing using three dansyl derivatives bearing a sulfur bridge

Frederico Duarte [a], Georgi Dobrikov [b,*], Atanas Kurutos [b,c], Jose Luis Capelo-Martinez [a,d], Hugo M. Santos [a,d], Elisabete Oliveira [a,d,*], Carlos Lodeiro [a,d,*]

[a] BIOSCOPE Research Group, LAQV-REQUIMTE, Chemistry Department, NOVA School of Science and Technology, FCT NOVA, Universidade NOVA de Lisboa, 2829-516 Caparica, Portugal
[b] Institute of Organic Chemistry with Centre of Phytochemistry, Bulgarian Academy of Sciences, Acad. G. Bonchev str., bl. 9, 1113 Sofia, Bulgaria
[c] University of Chemical Technology and Metallurgy, 8 St. Kliment Ohridski blvd, 1756 Sofia, Bulgaria
[d] PROTEOMASS Scientific Society, Departmental Building, BIOSCOPE Group laboratories, Ground Floor, FCT-NOVA Caparica Campus, 2829-516 Caparica, Portugal

ARTICLE INFO

Keywords:
Polymers
Dansyl derivatives
Metal ions
Sensors
Solvatochromism
Temperature

ABSTRACT

Three novel bis-dansyl derivatives bearing a sulfur bridge have been synthesized, fully characterized, and their photophysical characterization studied in solution, as well as, in the solid state. All compounds exhibit fluorescence emission with quantum yields up to 60%, which vary significantly depending on the solvent used, and the inherent molecular structure. Moreover, these compounds demonstrate positive solvatofluorochromic behaviour emitting from bluish-green to yellow. Kamlet-Taft studies were performed to better understand the solute–solvent interactions. Due to the intrinsic characteristics of the compounds, efforts were made to understand their potential usefulness for environmental remediation and thus metal ion sensing studies were investigated. Compounds **L1** and **L2** showed high sensitivity to Cu^{2+} and Hg^{2+} ions and were found to modulate their emission extensively, with **L2** capable of detecting and quantifying up to 4 μM of Hg^{2+}. Considering the solid-state emission of these compounds, the application towards temperature sensing was put forth. **L3** was found to quench its emission in a linear relation with temperature up to 170 °C. Several doped polymer thin films were fabricated, which served as a platform to establish a linear relation with temperature beyond their melting point. Polymethylmetacrylate (PMMA) films emitted up to temperatures of 218 °C, which could be fully restored at room temperature. These results suggest the potential application of these bis-chromophoric compounds as molecular thermometers.

1. Introduction

Probes and sensors conceptualized using fluorescent dyes offer inherent value due to their remarkable optical properties [1–3]. Among them, compounds based on 1-(dimethylamino)-naphthalene-5- sulfonyl or dansyl derivatives, have received consistent attention since they often exhibit broad emission spectra, high quantum yields and are robust enough under different external conditions [4–9]. This brought up to light a multitude of possible applications, ranging from biological targets such as the detection of oxygen reactive species [10], imaging [8,11–15], and monitoring of organ systems [6], to the detection of heavy and transition metal ions [12–20] and even water traces [4].

Our group has been working on metal ion detection for the last fifteen years [21–24]. Among them, the heavy and transition metal ions including Hg^{2+} and Cu^{2+} have gathered considerable attention. Hg^{2+} is a potential hazardous and toxic environmental pollutant that cause immunotoxic and neurotoxic effects in humans, leading to damage of the central nervous system and organ failure. On the other hand, Cu^{2+} is abundant in the body and plays a crucial role in diverse biological processes and cellular functioning. Abnormal concentration of Cu^{2+} may lead to the disruption of metabolic processes and neurodegenerative diseases such as Alzheimer's and Wilson diseases [14,17,25]. The U.S. Environmental Protection Agency has set admissible levels of Hg^{2+} and Cu^{2+} in drinking water to be 10 nM and 20 μM, respectively. Therefore, the development of fluorescent sensors for the detection of these transition metals is of utmost importance [12,17].

* Corresponding authors at: BIOSCOPE Research Group, LAQV-REQUIMTE, Chemistry Department, NOVA School of Science and Technology, FCT NOVA, Universidade NOVA de Lisboa, 2829-516 Caparica, Portugal.
E-mail addresses: Georgi.Dobrikov@orgchm.bas.bg (G. Dobrikov), ej.oliveira@fct.unl.pt (E. Oliveira), cle@fct.unl.pt (C. Lodeiro).

https://doi.org/10.1016/j.jphotochem.2023.115033
Received 23 May 2023; Received in revised form 20 July 2023; Accepted 22 July 2023
Available online 25 July 2023

Considering the constant search for improved sensors for metal ions, Anna Aliberti *et. al.* designed several dansyl-amino acids capable of detecting Hg^{2+}. Among them, N-dansylated methionine was the chemosensor that showed the best performance in terms of sensitivity, with a limit of detection (LOD) value of 140 nM. To improve the LOD of this chemosensor, a portable experimental set-up based on an optical fiber probe was developed, which was able to increase the LOD to 5 nM, meeting the requirements of the Environmental Protection Agency. However, application to water-based matrices was found to be unfruitful due to the coordinating ability of chloride anions towards Hg^{2+} [16]. Similarly, Bhawna Uttam *et. al.* developed a dansyl appended calix[4] arene on the lower rim, which selectively detected Hg^{2+} with a LOD value of 560 nM. MTT assay was performed using HeLa cells confirming its biocompatibility, and strong fluorescence was visualized by confocal microscopy. The removal of Hg^{2+} from water sources was also addressed by embedding the sensor on a zeolitic imidazolate framework with 5% encapsulation. ICP-MS studies suggested a 95% removal of Hg^{2+} from water using the hybrid metal–organic framework (MOF), displaying excellent selectivity even in the solid state [13].

On the other hand, the employment of dansyl derivatives towards sensing of Cu^{2+} ions have been put forward by Huie Jiang *et. al.* whom developed a novel fluorescent probe through a nucleophilic substitution reaction between dansyl chloride and 2-(piperazin-1-yl)ethanol at room temperature. The compound was found to be selective and sensitive for Cu^{2+} ions, causing the red shift and quenching of the emission and presented a low detection limit of 0.18 μM. Furthermore, this compound was successfully applied for the monitorization of Cu^{2+} ions in living cells particularly A549 cells using two-photon confocal fluorescence imaging [12]. Additionally, Rajendran Nagarajan *et. al.* have synthesized an unnatural amino acid-based phenylalanine that has been linked to dansyl and benzoxazole moieties. Competitive studies with other metal ions showed a selective quenching towards Cu^{2+} ions within aqueous organic media with physiological pH with a LOD value of 3.0 μM. Further water analysis studies indicated the usefulness of this compound being capable of recovering 99.92% of the Cu^{2+} ions in spiked tap and drinking water samples [25].

On the other hand, solvatochromism is another well-known and fairly common property among dansyl derivatives, as the dipole moment undergoes considerable changes as the solvent polarity increases, resulting in a significant Stokes shift [7,26–29]. However, further, research is needed to develop probes with high solvatochromism that do not succumb to aggregation-caused fluorescence quenching (ACQ) effects in hydrophilic and hydrophobic environments [8,30]. A more prevalent example of the contrast between these two types of environments is within cells, where different regions and organelles exhibit varying affinities for water. Na Li *et al.* have developed a robust polarity sensor to address this issue, which can track the decrease of lipid droplets when subjected to oxidative stress in live cells. The system involves the covalent bond between dansyl chloride and nile red derivative, capable of sensing polarity changes in both green and red detection channels. The fluorophore was found useful in both environments since the dansyl moiety was resistant to ACQ, while nile red changed the fluorescence in the red channel with high linearity of aqueous composition. This dual emission also provided the experimental results supporting the conclusion that oxidative stress leads to a sharp decrease in lipid droplets [8].

Fluorescent dye-doped solid support materials have generated great interest, as they have the potential to improve the intrinsic properties of the dye, such as stability against quenchers, sensitivity, fluorescence and prevention of aggregation-caused quenching (ACQ) [31,32]. These multifunctioning materials can be applied as sensors for pH [33,34], transition metals [17], temperature and smart materials [34–38] and even low-cost antibacterial polymers for biomedical and food packaging [39]. Given the diverse implementation of dansyl derivatives into multifunctional solid materials [31,40–42], and our recent knowledge on bis-dansyl derivatives bearing a disulfide bridge [43], the three dansyl derivatives **L1**, **L2** and **L3** bearing single sulfur bridges were synthesized and fully characterized. Above mentioned ligands were designed in order to demonstrate good complexation ability toward heavy metals. Presence of multiple amide bonds [44] as well as sulfur with aliphatic substituents in one molecule [45,46] ensure chelating effect of the ligands. Discovery of solvatochromic effect was accomplished alongside with their ability to sense pollutant metal ions, and incorporated into polymer thin films of polystyrene-block-polybutadiene-block-polystyrene (SBS), Poly(methylmethacrylate) (PMMA), Polyvinyl alcohol and poly(styrene–butadiene–styrene) copolymer (PVA:PVP) and thermoplastic polyurethane (TPU) towards the development of temperature-smart materials.

2. Experimental section

2.1. Materials

Spectroscopy grade solvents were used for photophysical experiments – ethanol (EtOH), toluene, tetrahydrofuran (THF), acetonitrile (CH_3CN), dimethylsulfoxyde (DMSO), dimethylformamide (DMF), chloroform ($CHCl_3$). Puriss. p.a. grade solvents were used after distillation for synthesis and purification of compounds – dichloromethane (DCM), petroleum ether (PE), methyl *tert*-butyl ether (MTBE), ethanol (EtOH).

Trifluoromethanesulfonate salts of Cu(II), Cd(II), Co(II), Ag(I), Pb(II), Zn(II), Ni(II) and Ca(II) have been obtained from Solchemar, while $Hg(OTf)_2$, dansyl amide and all solvents were purchased from Sigma Aldrich without the necessity of performing additional steps of purification. Poly(methylmethacrylate), PMMA (MW ~ 350,000, Tg 105 °C) polyvinylpyrrolidone, PVP (MW ~ 40,000, Tg 170 °C), Polyvinyl alcohol (PVA, MW 27,000, Tg 85 °C) and poly(styrene–butadiene–styrene), SBS (Styrene 30 wt%, Tg 95 °C) were purchased from Sigma-Aldrich (St. Louis, MO, USA). The perfluoroalkoxy (PFA) supports for the fabrication of polymer films were purchased to Bohlender, Gmbh, Germany. Mili-Q ultrapure water was used in all experiments. The thermoplastic polyurethane TPU-A92 was offered by Huntsman (Germany).

2.2. Instrumentation

Visualization of the TLC was performed using a Vilber UV Lamp (BVL-6.LC dual wavelength 254 nm/365 nm, operational power of 2 × 6 Watts).

Using a combination of ^1H NMR and ^{13}C NMR all compounds' chemical identities were verified. Using 5 mm tubes on a Bruker Avance II + 600 spectrometer, the ^1H NMR and ^{13}C NMR spectra were measured in $CDCl_3$ at 293 K at operating frequencies of 600.13 MHz and 150.92 MHz, respectively. ^1H and ^{13}C NMR spectra were calibrated to the signal of tetramethylsilane (TMS), $\delta = 0.00$. Chemical shifts are measured to an accuracy of 0.01 parts per million (ppm). The coupling constants (*J*) are shown with a precision of 0.1 and represented in Hz. The spin multiplicity in the 1H NMR was denoted by the abbreviations s = singlet, d = doublet, t = triplet, q = quartet, dd = doublet of doublets, dt = doublet of triplets, td = triplet of doublets, and m = multiplet.

High-Resolution Mass Spectrometry analyses have been performed in the Laboratory for Biological Mass Spectrometry–Isabel Moura (PROTEOMASS Scientific Society Facility), using UHR ESI-Qq-TOF IMPACT HD (Bruker-Daltonics, Bremen, Germany). Samples of the corresponding compounds were prepared by dissolution in 50% (v/v) Acetonitrile containing 0.1% (v/v) aqueous formic acid to obtain a working solution of 0.1 μg/mL. Mass spectrometry analysis was carried out by the direct infusion of the compound solutions into the ESI source. MS data were acquired in positive polarity over the mass range of 80–1300 *m/z*. (Capillary voltage: 4500 V, End plate offset: −500 V, Charging voltage: 2000 V, Corona: 4000 nA, Nebulizer gas: 0.4 Bar, Dry Heater: 180 °C, Dry gas: 4.0 L/min).

UV–Vis absorption spectra were recorded on a JASCO V-650 spectrophotometer and a fluorescence emission spectrum on a HORIBA Scientific FLUOROMAX-4 spectrofluorometer from BIOSCOPE-PROTEOMASS facilities.

2.3. Synthetic procedures

2.3.1. Synthesis of intermediates *3* and *6*

N,*N*'-(thiobis(ethane-2,1-diyl))bis(2-aminobenzamide) **(3)**:

In a 100 mL flask with 50 mL dry DCM were added consequently anthranilic acid (**2**) (2.51 g, 18.30 mmol, 2.2 eq.), diamine **1** (1.00 g, 0.95 mL, 8.32 mmol, 1.0 eq.), DIPEA (4.73 g, 6.05 mL, 36.60 mmol, 4.4 eq.) and TBTU (5.88 g, 18.30 mmol, 2.2 eq.). The formed clear solution was stirred at r.t. for 72 h. TLC of reaction mixture – DCM:MTBE = 5:1, x1. Workup: dilution with 30 mL DCM and washing with distilled water, aq. K_2CO_3 and again with water. The organic phase was dried over anhydr. Na_2SO_4, filtered, and evaporated to dryness. This crude product was recrystallized from EtOH:H_2O = 25:10 mL. The precipitate was filtered, washed with PE:MTBE = 30:10 and dried *in vacuo* to give 2.22 g (74%) of pure **3** as white-off powder. M.p. 121–122 °C. ^{1}H NMR (600 MHz, $CDCl_3$) δ 7.34 (dd, J = 7.9, 1.5 Hz, 2H), 7.20 (ddd, J = 8.4, 7.1, 1.5 Hz, 2H), 6.67 (dd, J = 8.2, 1.1 Hz, 2H), 6.65 – 6.60 (m, 4H), 5.48 (s, 4H), 3.62 (q, J = 6.2 Hz, 4H), 2.82 – 2.79 (m, 4H). ^{13}C NMR (151 MHz, $CDCl_3$) δ 169.61, 148.78, 132.53, 127.45, 117.44, 116.84, 116.01, 38.77, 31.83.

N^2,N^5-bis(2-aminobenzyl)thiophene-2,5-dicarboxamide **(6)**:

In a 100 mL flask with 50 mL dry DCM were added consequently diacid (**4**) (0.300 g, 1.74 mmol, 1.0 eq.), diamine **5** (0.45 g, 3.66 mmol, 2.1 eq.), DIPEA (1.24 g, 1.58 mL, 9.59 mmol, 5.5 eq.) and TBTU (1.23 g, 3.83 mmol, 2.2 eq.). The formed fine pale-yellow suspension was stirred at r.t. for 20 h. Workup: the solvent was evaporated, and the formed solid product was dispersed in hot water and filtered. This crude product was crystalized from EtOH:H_2O = 40:5 mL, filtered and dried *in vacuo* to give 0.46 g (69%) of pure **6** as white powder. M.p. 214–215 °C (with decomp.). ^{1}H NMR (600 MHz, DMSO-d_6) δ 9.07 (t, J = 6.0 Hz, 1H), 7.75 (s, 1H), 7.02 (dd, J = 7.5, 1.6 Hz, 1H), 6.97 (td, J = 7.6, 1.6 Hz, 1H), 6.62 (dd, J = 7.9, 1.2 Hz, 1H), 6.51 (td, J = 7.4, 1.2 Hz, 1H), 5.12 (s, 2H), 4.29 (d, J = 6.1 Hz, 2H). ^{13}C NMR (151 MHz, DMSO-d_6) δ 160.97, 146.27, 143.05, 129.25, 128.50, 128.10, 121.62, 115.91, 114.78.

2.3.2. Synthesis of *L1*, *L2* and *L3*

N,*N*'-(thiobis(ethane-2,1-diyl))bis(2-((5-(dimethylamino)naphthalene)-1-sulfonamido)benzamide) **(L1)**:

Compound **3** (0.250 g, 0.70 mmol, 1.0 eq.) was dissolved in 4 mL dry pyridine. Subsequently, dansyl chloride (0.452 g, 1.67 mmol, 2.4 eq.) was added and the formed clear solution was refluxed for 2 h. TLC of reaction mixture – DCM:MTBE = 5:1, x1. Workup: after cooling an excess of conc. aq. citric acid was added and extracted with DCM. The organic phase was washed with water, dried over anhydr. Na_2SO_4, filtered, and evaporated to dryness. This crude product was purified by column chromatography: 70 g silica, phase DCM:MTBE = 20:1. After evaporation of phase and drying *in vacuo*, pure **L1** was obtained as bright yellow powder (0.31 g, 54%). M.p. 111–112 °C. ^{1}H NMR (600 MHz, CDC**l3**) δ 11.25 (s, 2H), 8.46 (dt, J = 8.6, 1.1 Hz, 2H), 8.33 (dt, J = 8.7, 0.9 Hz, 2H), 8.24 (dd, J = 7.3, 1.3 Hz, 2H), 7.55 – 7.47 (m, 4H), 7.43 (dd, J = 8.5, 7.3 Hz, 2H), 7.27 (dd, J = 7.9, 1.5 Hz, 2H), 7.28 – 7.21 (m, 2H), 7.11 (dd, J = 7.6, 0.9 Hz, 2H), 6.81 (td, J = 7.6, 1.2 Hz, 2H), 6.65 (t, J = 5.9 Hz, 2H), 3.44 (q, J = 6.4 Hz, 4H), 2.81 (s, 12H), 2.66 (t, J = 6.5 Hz, 4H). ^{13}C NMR (151 MHz, CDC l_3) δ 168.77, 151.91, 138.86, 134.80, 132.67, 130.91, 130.05, 129.93, 129.61, 128.51, 127.02, 123.13, 123.05, 120.62, 119.76, 119.12, 115.41, 45.51, 39.03, 31.50. ESI-MS: $[M + H]^+$ for $C_{42}H_{44}N_6O_6S_3$ = 825.2552 (-0.6 ppm), and $[M + 2H]^{2+}$ for $C_{42}H_{44}N_6O_6S_3$ = 413.1307 (-1.9 ppm). Calculated $[M + H]^+$ for $C_{42}H_{44}N_6O_6S_3$ = 825.255723 and $[M + 2H]^{2+}$ for $C_{42}H_{44}N_6O_6S_3$ = 413.131500.

N,*N*'-(thiobis(ethane-2,1-diyl))bis(5-(dimethylamino)naphthalene-1-sulfonamide) **(L2)**:

Diamine **1** (0.089 g, 0.085 mL, 0.74 mmol, 1.0 eq.) and DIPEA (0.240 g, 0.32 mL, 1.85 mmol, 2.5 eq.) were dissolved in 50 mL dry DCM and cooled to 5 °C (with ice-water). Then dansyl chloride (0.400 g, 1.48 mmol, 2.0 eq.) was added in one portion and the formed clear mixture was stirred for 30 min at 5 °C, followed by 48 h at r.t. TLC of reaction mixture – DCM:MTBE = 10:1, x1. Workup: dilution with 30 mL DCM and washing with 1% aq. citric acid and water. The organic phase was dried over anhydr. Na_2SO_4, filtered and evaporated to dryness. This crude product was purified by column chromatography: 70 g silica, phase DCM:MTBE = 20:1. After evaporation of phase and drying *in vacuo*, pure **L2** was obtained as pale-yellow powder (0.20 g, 46%). M.p. 70–71 °C. ^{1}H NMR (600 MHz, CDC**L3**) δ 8.53 (d, J = 8.5 Hz, 2H), 8.24 (d, J = 8.6 Hz, 2H), 8.20 (dd, J = 7.3, 1.3 Hz, 2H), 7.54 (dd, J = 8.6, 7.5 Hz, 2H), 7.50 (dd, J = 8.5, 7.3 Hz, 2H), 7.17 (d, J = 7.5 Hz, 1H), 2.88 (s, 16H), 2.25 (t, J = 6.4 Hz, 4H). ^{13}C NMR (151 MHz, $CDCl_3$) δ 152.18, 134.53, 130.78, 129.96, 129.78, 129.59, 128.69, 123.32, 118.69, 115.41, 45.55, 42.00, 31.42. ESI-MS: $[M + H]^+$ for $C_{28}H_{34}N_4O_4S_3$ = 587.1811 (-0.7 ppm). Calculated $[M + H]^+$ for $C_{28}H_{34}N_4O_4S_3$ = 587.181495.

N^2,N^5-bis(2-((5-(dimethylamino)naphthalene)-1-sulfonamido) benzyl)thiophene-2,5-dicarboxamide **(L3)**:

Compound **6** (0.300 g, 0.79 mmol, 1.0 eq.) was dissolved in 5 mL dry pyridine. Then dansyl chloride (0.468 g, 1.73 mmol, 2.2 eq.) was added and the formed clear solution was stirred at r.t. for 72 h. TLC of reaction mixture – DCM:MTBE = 5:1, x2. Workup: excess of conc. aq. citric acid was added and extracted with DCM. The organic phase was washed with water, dried over anhydr. Na_2SO_4, filtered, and evaporated to dryness. This crude product was purified by column chromatography: 70 g silica, phase 1 - DCM:MTBE = 10:1 (for contaminations); phase 2 - DCM:MTBE = 5:1 (for product). After evaporation of phase and drying *in vacuo*, pure **L3** was obtained as pale-yellow powder (0.51 g, 76%). M.p. 263–264 °C. ^{1}H NMR (600 MHz, DMSO-d_6) δ 10.24 (s, 2H), 9.23 (t, J = 6.1 Hz, 2H), 8.47 (dt, J = 8.5, 1.1 Hz, 2H), 8.42 – 8.36 (m, 2H), 8.09 (dd, J = 7.3, 1.3 Hz, 2H), 7.76 (s, 2H), 7.57 (ddd, J = 11.9, 8.6, 7.4 Hz, 4H), 7.24 (dd, J = 7.7, 0.9 Hz, 2H), 7.20 – 7.15 (m, 2H), 7.12 – 7.05 (m, 4H), 6.90 – 6.85 (m, 2H), 4.32 (d, J = 6.1 Hz, 4H), 2.81 (s, 12H). ^{13}C NMR (151 MHz, DMSO-d_6) δ 161.39, 151.61, 142.64, 135.47, 134.49, 133.19, 130.31, 129.56, 129.07, 129.04, 128.27, 127.97, 125.91, 124.11, 123.69, 118.77, 115.35, 45.14. ESI-MS: $[M + H]^+$ for $C_{44}H_{42}N_6O_6S_3$ = 847.2389 (-1.3 ppm), and $[M + 2H]^{2+}$ for $C_{42}H_{42}N_6O_6S_3$ = 424.1245 (1.9 ppm). Calculated $[M + H]^+$ for $C_{44}H_{42}N_6O_6S_3$ = 847.240073, and $[M + 2H]^{2+}$ for $C_{42}H_{42}N_6O_6S_3$ = 424.123674.

2.4. Spectrophotometric and spectrofluorimetric measurements

2.4.1. Photophysical characterization and titrations

Photophysical characterizations and titrations were performed by preparation of stock solutions of compounds **L1**, **L2** and **L3** (ca. 10^{-3} M) in different solvents (CH_3CN, EtOH, DMSO, $CHCl_3$, Toluene, THF and DMF), by dissolution of an appropriate amount of the selected compound in a 10 mL volumetric flask. Further studies were carried out by appropriate dilution of the stock solutions up to 10^{-5} – 10^{-6} M.

Titrations of **L1** and **L2** were carried out by the addition of microliter aliquots of standard solutions of Ca^{2+}, Co^{2+}, Ni^{2+}, Cu^{2+}, Zn^{2+}, Ag^+, Cd^{2+}, Hg^{2+}, Pb^{2+} ions prepared in acetonitrile, while titrations of **L3** were carried out in DMSO. A correction for the absorbed light was performed when necessary. Luminescence spectra of the compounds in the solid state and of doped polymer thin films were recorded using of a fiber-optics device connected to the spectrofluorometer while exciting the samples at appropriated wavelength. The temperature dependent emission spectra were recorded by heating the samples over a hotplate with control over the temperature.

2.4.2. Fluorescence quantum yield and lifetime

Relative photoluminescence quantum yields were measured using

dansyl amide in acetonitrile employed as a standard solution ($\phi_F = 0.37$) for quantifying the relative QY of **L1** and **L2** dissolved in the same solvent and in DMSO for **L3**, while the remaining ones were measured relative to the standard solution of dansyl amide in DMSO ($\phi_F = 0.61$) [47]. Tempro Fluorescence Lifetime System with a Nanoled pulsed diode controller from Horiba Jobin-Yvon (Proteomass Facilities) was used to perform lifetime measurements.

2.5. Determination of the detection and quantification limits (LOD and LOQ)

Determination of the detection limit (LOD) and quantification limit (LOQ) began by collecting ten independent measurements of a solution containing the selected probe and no addition of any metal ion (y_{blank}). Final determination of the LOD and LOQ values followed the subsequent formulas [48,49]:

LOD = $y_{dl} = y_{blank} + 3std$, where y_{dl} = signal detection limit and std = standard deviation.

LOQ = $y_{dl} = y_{blank} + 10std$, where y_{dl} = signal detection limit and std = standard deviation.

The final step involved the determination of the minimal detectable and quantified concentration of metal ion by titration with the ligands.

2.6. Preparation of polymer Dye-Doped thin films

PMMA and SBS doped polymer thin films were obtained by slow evaporation of a 10 mL chloroform solution containing 100 mg of the corresponding polymer matrix and 0.5 mg of the selected compound.

PVA:PVP polymer films were prepared by dissolution of 200 mg of PVA and 50 mg of PVP in 1.5 mL miliQ water, while heating at 80 °C, with continuous stirring and 0.5 mg of the dansyl dyes were dissolved in 2 mL of EtOH and added to the hot mixture.

TPU doped polymer films were fabricated by dissolving 100 mg of the polymer matrix and 1 mg of the corresponding compounds in 10 mL of THF.

All mixtures were poured onto PFA supports with diameter of 5 cm to allow solvent evaporation at room temperature. All polymeric samples were prepared in triplicate.

3. Results and discussion

3.1. Synthesis

The synthesis of target compounds **L1** and **L2** was based on commercially available thio-diamine **1** (Scheme 1). Preparation of intermediate **3** was accomplished by direct coupling reaction of **1** with anthranilic acid (**2**). Due to better nucleophilicity of amino groups of **1**, preparation of **3** was performed in only one step and isolated with good yield without need of protection. Consequently, acylation of **3** with dansyl chloride in dry pyridine furnished the target product **L1** in good yield. The synthesis of compound **L2** was performed in one step starting from **1** and dansyl chloride, employing classical conditions (Et_3N in dry dichloromethane).

The preparation of ligand **L3** was conducted in two steps (Scheme 2). Intermediate **6** was prepared in one step from commercially available diacid **4** and diamine **5**, respectively. As in case of **3**, protection of **5** was not necessary. Acylation of **6** with excess of dansyl chloride in dry pyridine yields product **L3**. All intermediates and target compounds were obtained in good yields and high purity after column chromatography. They were fully characterized by NMR, MS and melting point temperatures.

3.2. Photophysical characterization

The dansyl derived compounds exhibit luminescence properties both in solution and in the solid state. Fig. 1 displays the molecular structure alongside the photophysical data collected at 298 K for compound **L1** and **L2** in acetonitrile as well as in DMSO for **L3** as a representative example. The UV–Vis spectra show a band centered at 330, 340 and 350 nm; associated with the π-π* transition of the dansyl chromophore, contributing to the visualization of colourless solutions in the naked eye. Upon excitation at the appropriate wavelength, the samples emit a greenish yellow light with a maxima at 524, 518 and 532 nm representative of a large stoke shift. On a relatable note, solid-state emission spectra show a wide band centered at 509, 499 and 469 nm, a considerable blue shift in relation to the emission in solution (Table 2).

Since dansyl derivatives are commonly associated with solvatochromism behavior, **L1**-**L3** were further studied for their photophysical properties in five different solvents to evaluate the sensitivity towards solvent polarity. Alongside in acetonitrile, **L1** and **L2** were

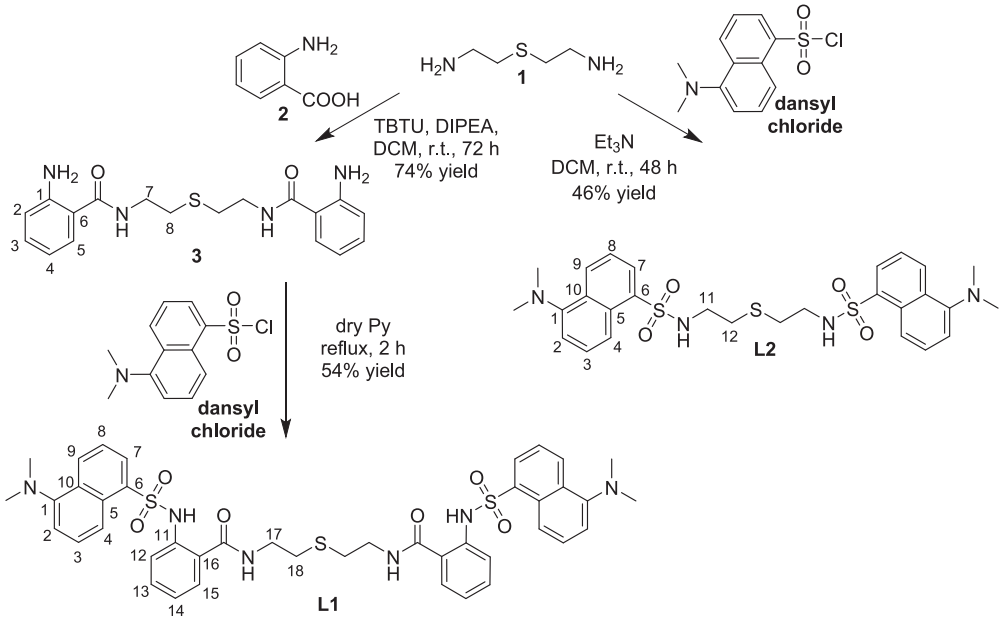

Scheme 1. Synthetic approach to the preparation of compounds **L1** and **L2.**

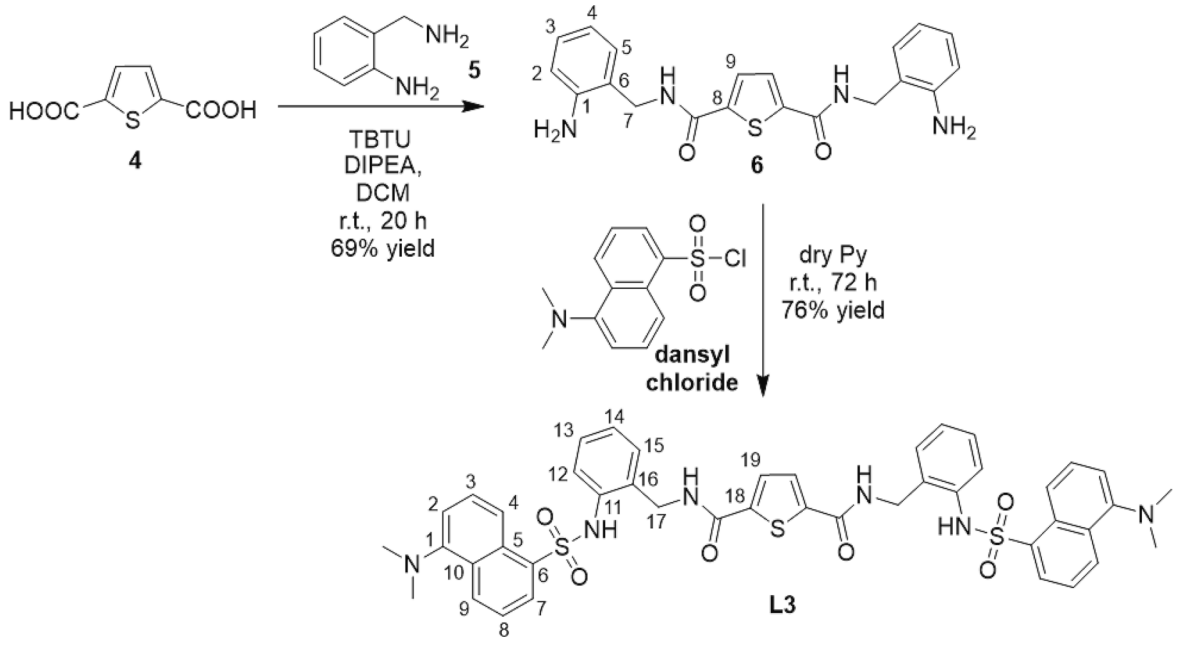

Scheme 2. Synthetic approach to the preparation of compound **L3.**

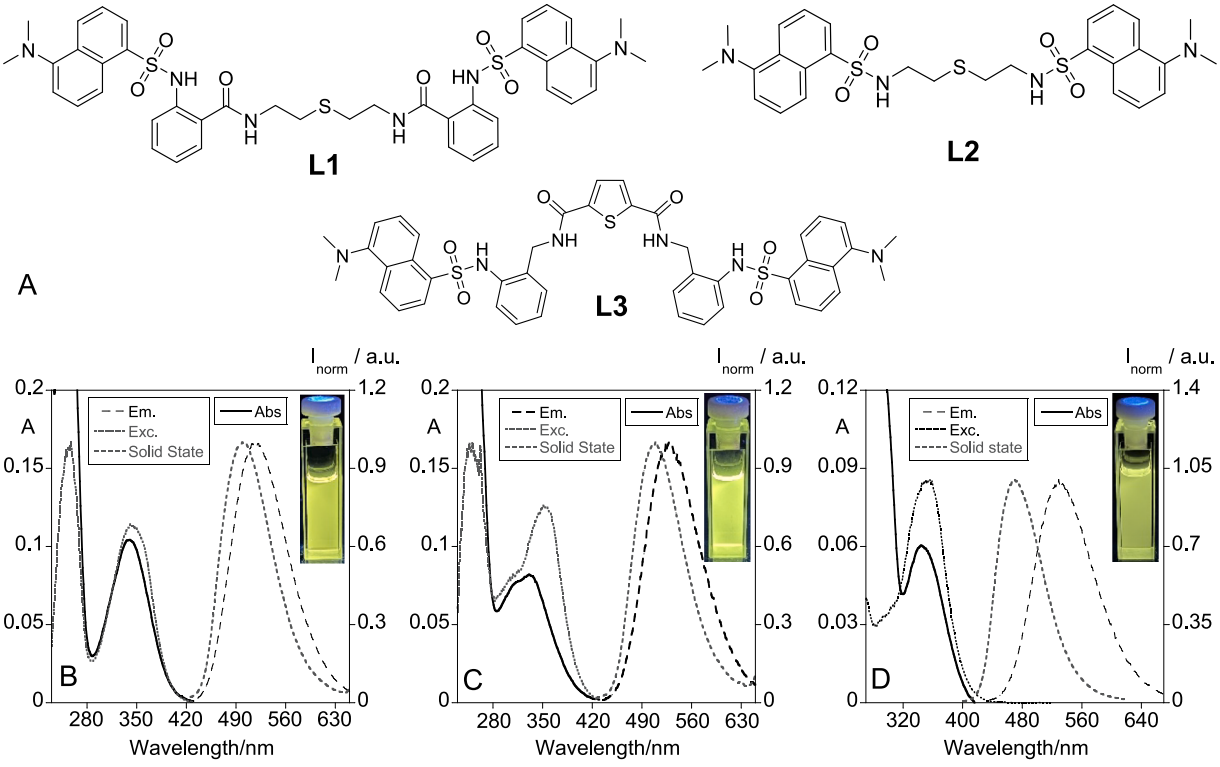

Fig. 1. (A) Molecular structure of dansyl based compounds **L1**, **L2** and **L3**. Photophysical characterization of derivatives **L1** (B), **L2** (C) in acetonitrile and **L3** (D) in DMSO ([**L1**] = [**L2**] = [**L3**] = 6 μM).

further studied in DMSO, ethanol, THF, chloroform and toluene; Due to solubility restrictions **L3** was studied in THF and DMF (Figs. S14–S18).

Taking into consideration the analysis of Table 3, no correlation can be perceived following the absorption as the solvent polarity increases despite the differences in maximum bands. On the contrary, the same cannot be said for the emission, where a clear red shift of the emission maximum bands is seen, a shift from 500 to 536 nm for **L1**, from 489 to 520 nm for **L2** and from 339 to 350 nm for **L3** with increasing solvent polarity. In line with these findings, a conclusion can be taken based on the shifts observed regarding the emission spectra, demonstrating that **L1**, **L2** and **L3** exhibit a positive solvatofluorochromism.

To fully characterize **L1** and **L2's** solvatofluorochromic behaviour, and to quantify the solute–solvent interactions, three solute-dependent parameters (υ_0, a, b and p) have been determined through the multi-parametric fitting of the kamlet-Taft equation (Equation (1)).

Table 1
Spectroscopic polarity parameters, physical properties of the different solvents. ε_r: relative permittivity; η: refractive index; α: the solvent's HBD acidity; β: the solvent's HBA basicity; π*: the solvent's dipolarity/polarizability.

Solvent	ε_r	α	β	π*	η
DMSO	47.24	0	0.76	1	1.47
DMF	38.4	0	0.69	0.88	1.43
CH_3CN	35.94	0.19	0.40	0.66	1.34
Ethanol	24.30	0.86	0.75	0.54	1.36
THF	7.58	0	0.55	0.58	1.40
$CHCl_3$	4.89	0.20	0.10	0.69	1.44
Toluene	2.38	0	0.11	0.54	1.49

$$\upsilon = \upsilon_0 + a\alpha + b\beta + p\pi^* \quad (1)$$

Where υ_0 represents the wavenumber value without dependence of solvent effects; parameters a, b and p are obtained through multiple regression analysis that reflect the underlying sensitivity of the probes photophysical behaviour to solvent polarity; α: hydrogen bond donor acidity (HBD); β: hydrogen bond acceptor basicity (HBA); π*: stabilization of a charge or dipole without a specific dielectric interaction (Table 1) [29,50].

Fig. 2 gathers the images taken under UV light lamp of **L1** and **L2** under a UV light lamp while Table 4 presents the fitted parameters (υ0, a, b and p) driven from the multiple regression analysis while the slope and correlation were obtained from the linear fitting of the plot $\upsilon_{exp.}$ versus $\upsilon_{calc.}$

From Table 4 it is perceived that **L3** has the highest polarizability making it more likely to be distorted by an external field.

3.3. Metal ions sensing

Keeping in mind the potential value of these dansyl derivatives to be used towards the sensing of metal ions, additions of 1, 5 and 10 equivalents of Ca^{2+}, Co^{2+}, Ni^{2+}, Cu^{2+}, Zn^{2+}, Ag^{+}, Cd^{2+}, Hg^{2+} and Pb^{2+} in acetonitrile were performed. Fig. 3 gathers the normalized emission intensities at 524, 518 and 532 nm of compounds **L1**-**L3**, respectively, upon addition of the aforementioned metal ions. Compounds **L1** and **L2** showed sensitivity towards Cu^{2+} and Hg^{2+} metal ions while **L3** hasn't been found to have any meaningful variation on its emission after addition of 10 equivalents of each metal most likely due to the inherent rigidity of the system.

In face of the previous results, Fig. 4 gathers the UV–Vis and luminescent titrations towards increasing amounts of Cu^{2+} (A, C) and Hg^{2+} (B, D) for **L1** and **L2**, respectively. Overall, the addition of both metal ions causes the continuous decrease of the absorbance maxima centered

Table 4
Independent fluorescence wavenumber ($\upsilon 0$), solvent polarity (p), HBD (a), HBA (b), slope and coefficient (R^2) of the linear fitting plot $\upsilon_{exp.}$ versus $\upsilon_{calc.}$

	υ_0	a	b	p	Slope	R^2
L1	21,144	−421	−721	−1848	0.99	0.99
L2	21,790	−1032	−299	−2314	0.99	0.99
L3	21,646	−1033	−301	−2626	0.99	0.99

Table 2
Absorption maximum wavelength in solution (λ_{abs}), emission maximum wavelength in solution (λ_{em}), molar absorption coefficients (ε), Stokes shift (Δλ), emission maximum in the solid state (λ_{em}^{Solid}), fluorescence quantum yields (ϕ), brightness (εxϕ), fluorescence lifetimes (τ) for compounds **L1** and **L2** in acetonitrile and **L3** in DMSO.

Cp.	λ_{abs} [nm]	λ_{em} [nm]	ε [10^4 cm^{-1} M^{-1}]	Stokes shift [10^4 cm^{-1}]	λ_{em}^{Solid} [nm]	ϕ (%)	Brightness (ε X ϕ) [10^3 cm^{-1} M^{-1}]	τ[ns]
L1	330	524	0.991	5.15	509	27	2.68	11
L2	340	518	1.06	5.62	499	35	3.71	12
L3	350	532	1.03	5.49	469	10	1.03	5.9

Table 3
Photophysical characterization of probes **L1** and **L2** performed in different organic solvents.

Cpd.	Solv.	λ_{abs} [nm]	λ_{em} [nm]	ε [10^4 cm^{-1} M^{-1}]	Stokes shift [10^4 cm^{-1}]	ϕ (%)	Brightness (ε X ϕ) [10^3 cm^{-1} M^{-1}]	τ[ns]
L1	DMSO	350	534	0.999	5.43	24	2.40	14
	EtOH	334	520	0.804	5.38	17	1.37	13
	THF	336	507	1.19	5.85	47	5.59	14
	$CHCl_3$	345	506	1.07	6.21	51	5.36	15
	Toluene	343	500	0.816	6.37	51	4.16	13
L2	DMSO	340	520	0.956	5.56	48	4.59	12
	EtOH	335	515	0.964	5.56	33	3.18	15
	THF	336	492	1.21	6.41	52	6.29	13
	$CHCl_3$	343	500	0.802	6.37	60	4.81	13
	Toluene	341	489	0.899	6.76	53	4.77	16
L3	DMF	336	523	1.16	5.35	3.6	0.428	7.7
	THF	339	501	1.34	6.17	7.3	0.978	6.6

Fig. 2. Images of **L1** (1–6), **L2** (7–12) and **L3** (13–15) in different organic solvents [Toluene (1,7); THF (2, 8, 13); Chloroform (3, 9); Acetonitrile (4, 10); Ethanol (5, 11); DMF (14); DMSO (6, 12, 15)] under a UV lamp.

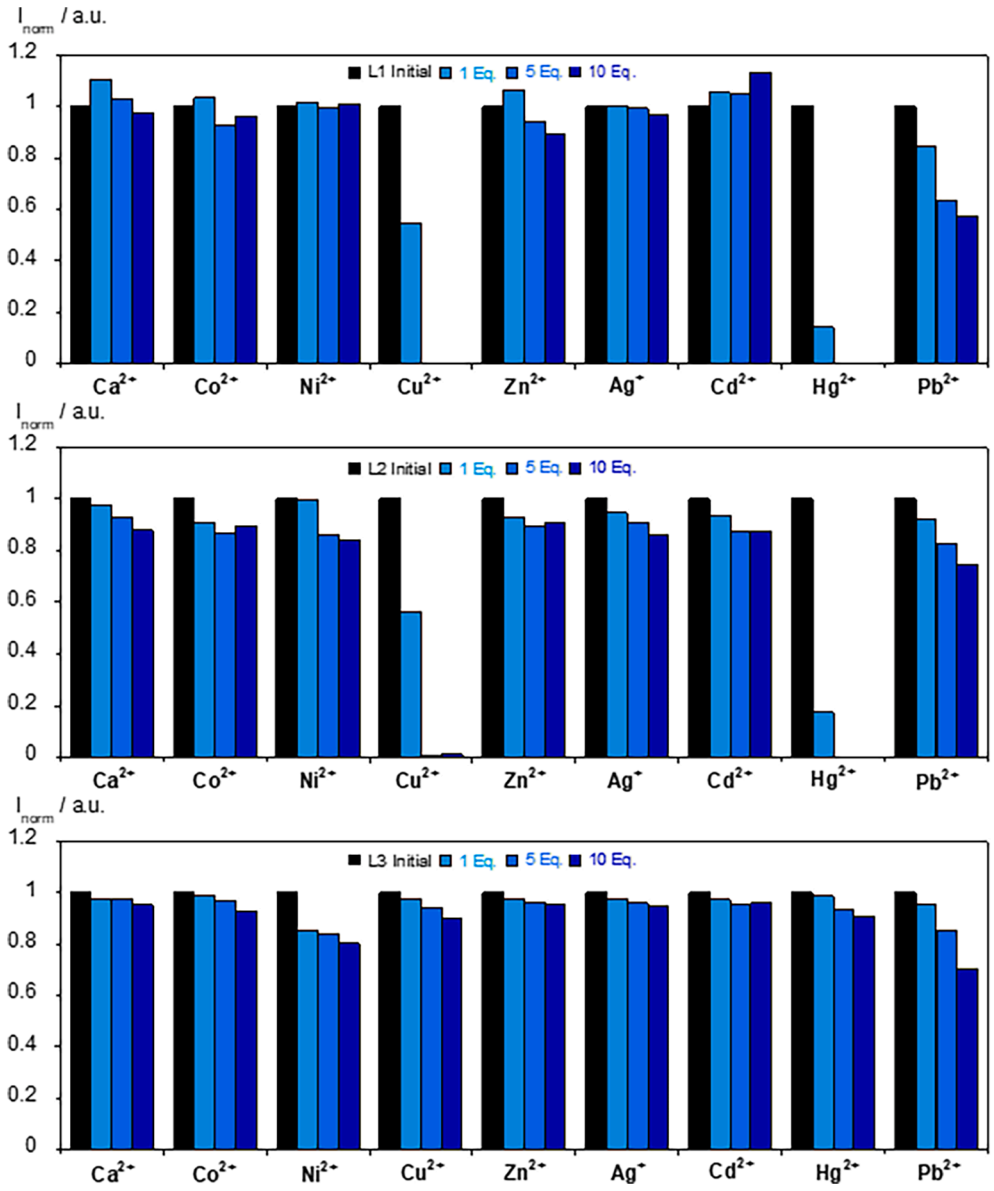

Fig. 3. Normalized emission intensity of **L1** (A), **L2** (B) and **L3** (C) after addition of Ca^{2+}, Co^{2+}, Ni^{2+}, Cu^{2+}, Zn^{2+}, Ag^{+}, Cd^{2+}, Hg^{2+} and Pb^{2+} metal ions in successive proportions of 1, 5, and 10 equivalents in acetonitrile for **L1** and **L2** while in DMSO for **L3**. ([**L1**] = [**L2**] = [**L3**] = 20 μM, λ_{emL1} = 524 nm, λ_{emL2} = 518 nm, λ_{emL3} = 532 nm, T = 298 K).

at 330 and 340 nm for **L1** and **L2**, respectively, while simultaneously a gradual formation of a band with a maximum around 300 nm is observed for both compounds, followed by the appearance of an additional band located around 370 nm in particular for **L2** when added Hg^{2+}. In terms of the emission spectra, a quenching on its intensity is observed in both cases at 524 (**L1**) and 518 nm (**L2**).

To fully characterize the sensing ability towards Cu^{2+} and Hg^{2+}, the stability constants were calculated with the aid of HypSpec software [51] alongside calculation of the detection and quantification limit parameters for both dansyl derivatives. The association constants, LOD and LOQ are included in Table 5.

Table 5 reveals that both probes assemble in mononuclear species with Cu^{2+} and Hg^{2+} with the highest constant belonging to **L2** towards Hg^{2+} with a stability constant value of $LogK_{ass.} = 6.38 \pm 0.02$. Ligand **L2** has also been found to exhibit the lowest LOD and LOQ values (4 μM and 7 μM) being indicative of a higher affinity to bind with Hg^{2+} ions. These results highlight the potential usefulness of this probe in environmental remediation of Hg^{2+} ions where there is the need to monitor its presence in lower concentrations.

Regarding compound **L1**, the lower stability constants found for this compound may be due to the increased stereochemical hindrance promoted by the addition of the benzene moiety which in turn disables to some degree the accessibility for the coordination to occur.

3.4. Studies using solid support compound L1

L1 in water offers an advantage when considering future practical applications. **L1** exhibits the lowest detection and quantification limit for Hg^{2+} metal ions in solution, making it suitable for supporting on low-cost, simple cellulose discs for the determination of Hg^{2+} in aqueous solutions.

Blank discs (*Liofilchem*) with a diameter of 6 mm were impregnated with a solution of **L1** ([**L1**] = 10 μM) in THF. After drying, the resulting white discs containing **L1** were briefly immersed for 5 s in water solutions with increasing concentrations of Hg^{2+} (0, 25, 50, 100, 200, 300, and 400 ppm). Fig. 5 illustrates the visual colour emission changes under

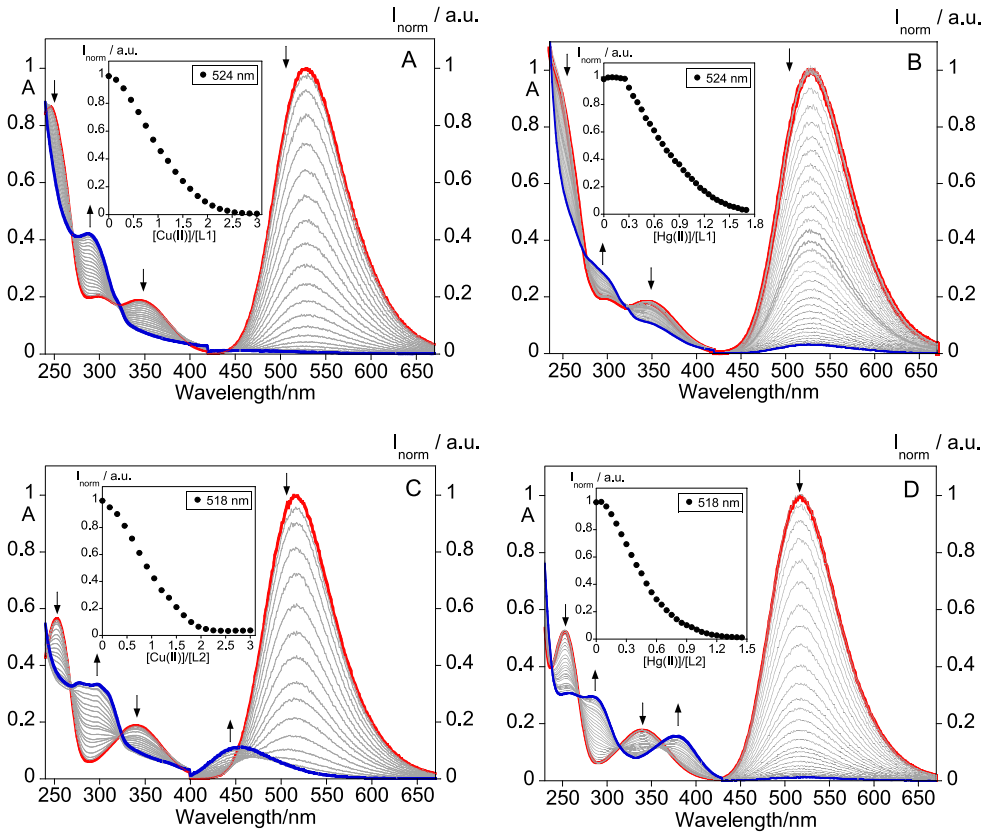

Fig. 4. UV–Vis and luminescent titrations of compounds **L1** (A, B) and **L2** (C, D) upon continuous addition of 10 μL of Cu^{2+} (A, C; $[Cu^{2+}] = 0.9$ mM), and Hg^{2+} (B, D; $[Hg^{2+}] = 0.3$ mM) in acetonitrile. The inset represents the emission (A-D) as a function of $[Cu^{2+}]/[\mathbf{L1}]$ at 524 nm (A), of $[Cu^{2+}]/[\mathbf{L2}]$ at 518 nm (C), of $[Hg^{2+}]/[\mathbf{L1}]$ at 524 nm (B) and of $[Hg^{2+}]/[\mathbf{L2}]$ at 518 nm (D). $[\mathbf{L1}] = [\mathbf{L2}] = 20$ μM, $\lambda_{exc\mathbf{L1}} = 330$ nm, $\lambda_{exc\mathbf{L2}} = 340$ nm, T = 298 K).

Table 5
HypSpec's calculated association constants and stoichiometry for the probes **L1** and **L2** towards Cu^{2+} and Hg^{2+} ions, in CH_3CN alongside the respective values for the Minimal detectable (LOD) and quantified (LOQ) amounts (μM). LOD and LOQ were measured by the emission at 524 and 518 nm for **L1** and **L2**, respectively.

Compounds	Metal (M)	Association constants ($LogK_{ass.}$), L:M	LOD (μM)	LOQ (μM)
L1	Cu^{2+}	4.82 ± 0.03 (1:1)	6	15
	Hg^{2+}	5.29 ± 0.06 (1:1)	7	11
L2	Cu^{2+}	5.00 ± 0.04 (1:1)	6	15
	Hg^{2+}	6.38 ± 0.02 (1:1)	4	7

a UV lamp. Notably, a visual detection of Hg^{2+} in water is possible from concentrations as low as 100 ppm. This method holds great potential for the development of portable and convenient in-the-field detection of Hg^{2+}.

3.5. Tuning the emission of dansyl derivatives towards temperature smart materials

Since **L1**-**L3** were found to exhibit emission in the solid state and manifest solvatofluorochromism due to the different properties of the solvents, the next intention is to modulate the emission of these ligands in solid supported materials to develop molecular thermometers through emission. In line with this premise, the compounds have been studied initially without the use of a solid supports. For this, emission of each probe has been recorded with the increase of temperature in the solid state. Fig. 6 gathers the emission spectra and the plot of I_{nom} in relation to temperature for compound **L3**. The results suggest that **L3** manifests a linear relation of its emission and the increase of temperature between 30 and 129 °C. The same behavior was also found during the cooling cycle. This compound was found to completely recover its emission by the end of the cooling cycle as it can be seen in Fig. 6.

Regarding compound **L1** and **L2**, a relation has been found between emission and temperature for **L1** between 30 and 70 °C while no linearity was observed for **L2** as can be seen in Figs. S19 and S20. Also, after cooling the emission did not recover substantially suggesting partial degradation of both compounds. This is most likely due to their low melting point around 112 and 70 °C for compound **L1** and **L2**, respectively. The same was not found for compound **L3** since its melting point is 264 °C. Thus, **L1** and **L3** have shown promising results allowing them to be used as temperature sensors, however applications may be hindered due to the lack of solid supports.

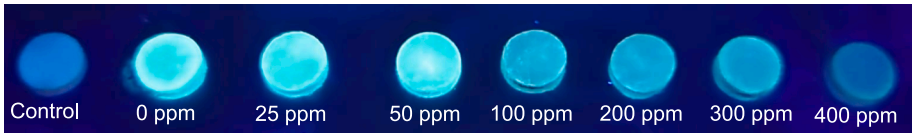

Fig. 5. Visual changes in Blank Discs (*Liofilchem*) containing compound **L1** (10 μM) after immersion in water solutions containing increasing concentrations of Hg^{2+} metal ion (0–400 ppm). [25 ppm = 50 μM; 50 ppm = 100 μM; 100 ppm = 200 μM; 200 ppm = 401 μM; 300 ppm = 602 μM; 400 ppm = 802 μM].

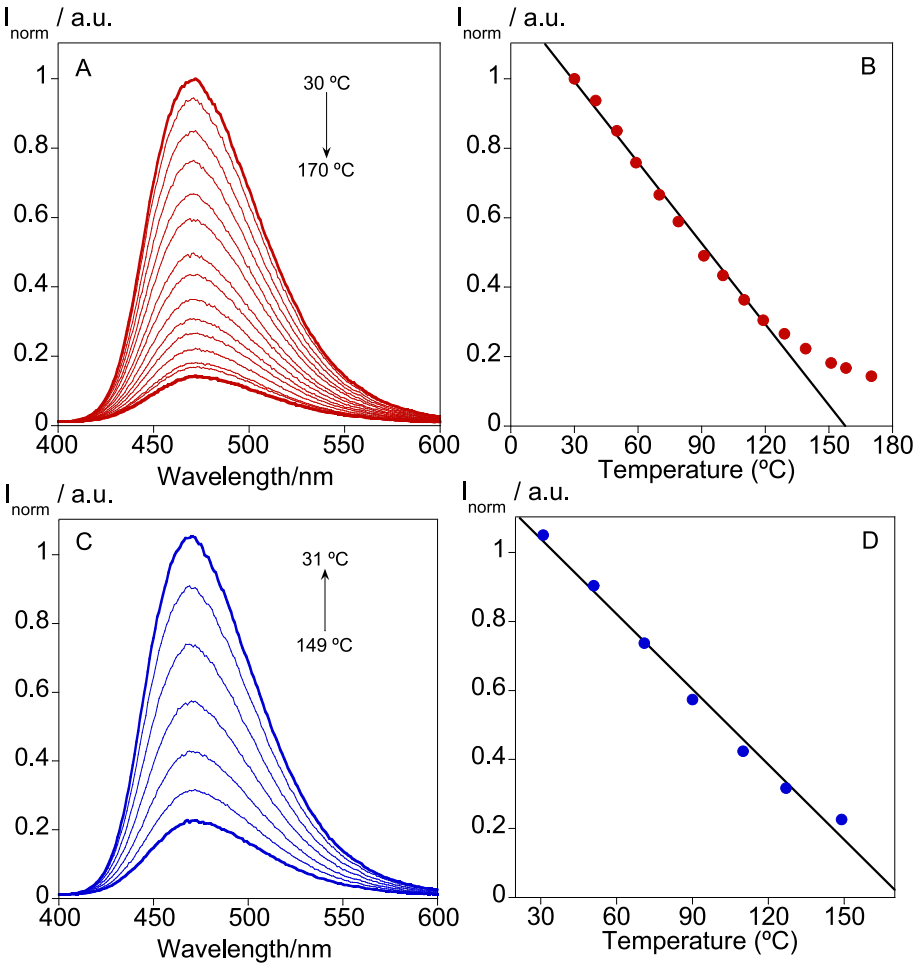

Fig. 6. Temperature-dependent emission spectra of **L3** in the solid state (A) collected through a warming cycle between 30 °C and 170 °C. I_{norm}. vs. T plot recorded in the emission maximum at 472 nm upon heating (B) [30 to 129 °C (Y = 1.2243 + 0.0077612x), yielding R = 0.99663]. Temperature-dependent emission spectra of **L3** (C) collected through a cooling cycle between 31 °C and 149 °C. I_{norm}. vs. T plot recorded in the emission maximum at 472 nm upon cooling (D) [31 to 149 °C (Y = 1.2571 + 0.0072628x), yielding R = 0.99502].

According with the previous findings, several polymers doped thin films have been developed as a next step to improve the sensing applications. Compound **L1** and **L2** were doped in PMMA, SBS, PVA:PVP and TPU while **L3**, due to solubility restrictions, has been doped only in TPU. Fig. 7 gathers the comparison between the emission spectra in the solid state and each emission of the different polymer thin films while Table 6 presents the corresponding emission maximum.

Overall, polymer thin films were successfully developed, and their emission properties were investigated. As it can be perceived by Fig. 7, the molecular structure of the polymer matrix is able to tune the final emission of the film by interacting with the probe. PMMA films display the largest blue-shift of 37 and 32 nm for **L1** and **L2**, respectively, without relevant input of the differences in molecular structure of both probes. However, for SBS and PVA/PVP more pronounced differences are observed due to the influence of the molecular structure. Compound **L1** tends to suffer less relevant blue-shifts on these polymer matrixes than **L2** most likely due to the increased compatibility that the benzene moieties provide while dispersed. Regarding TPU polymer thin films of **L1** and **L2**, blue shifts of 16 and 12 nm are observed. Nevertheless, the most interesting appears to be **L3** that when doped originates a red shift of 22 nm.

In face of the previous results, each polymer doped films were studied with variation in temperature aiming to better understand whether it is possible to humper the constrains that were found in the solid state for **L1** and **L2**. Fig. 8 gathers the emission of the different polymer films doped with **L2**, as a representative example, alongside **L3** doped in TPU polymer film while polymer doped films of **L1** can be seen in Figs. S21–S24.

Regarding the PMMA doped film, this material suffers its quenching with increments of temperature up to 218 °C. Intriguingly, the behaviour observed for **L1** and **L2** in the solid state, due to their melting point, does not influence to the same extent the emission in the solid support. The polymer matrix serves as a media to maintain the emission at higher temperatures by providing sufficient conductivity which attenuates the thermal activated non-radiative processes that the compounds manifest. Likewise, as the cooling stage proceeds the emission gradually increases until it reaches room temperature and is capable of recovering 85% of the initial fluorescence. Additionally, linearity can be perceived from 120 to 218 °C during heating and until 51 °C while cooling. It is also, interesting to note that the glass transition temperature of PMMA (T_g 105 °C) do not seem to have any influence in the emission behaviour of the film.

Remaining polymer supports were able to provide similar behaviour in relation to the emission properties with temperature. However, were not able to reach the same temperatures as PMMA and have been also found to not recover substantially their emission when cooled to room temperature (Fig. S25) since they start to experience physical changes. On the other hand, linearity of the emission with temperature can still be perceived for SBS, PVA/PVP, and TPU between 70 to 189 °C, 110 to 199 °C and 70 and 158 °C.

In the case of TPU doped with **L3**, the quenching of the emission is observed similarly as observed for the solid state, however linearity can only be seen between 80 and 159 °C, while during cooling emission recovers 40% and shows linearity between 33 and 148 °C (Fig. S26). Nevertheless, in agreement with the other doped polymer materials studied, the incorporation of the probe onto a solid support provides the means to be applied as a molecular thermometer without restrictions imposed by their physical characteristic and, in this particular case, the

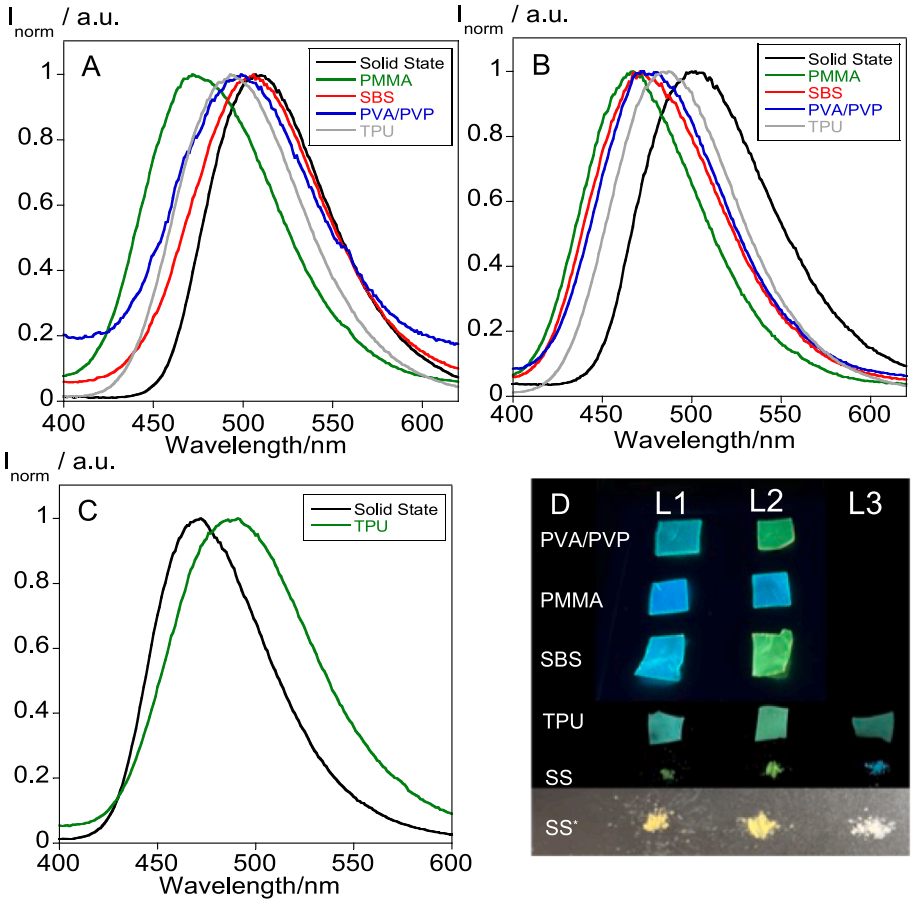

Fig. 7. Comparison between the emission spectra of the different polymer thin films doped with (A) L1, (B) L2 and (C) L3 and the respective emission spectrum in the solid state. Images of the different polymer doped films and in the solid state under UV-light and under natural light (*) (D).

Table 6
Emission maximum in the solid state (λ_{em}^{Solid}), emission maximum of PMMA thin films (λ_{em}^{PMMA}), emission maximum of SBS thin films (λ_{em}^{SBS}), emission maximum of PVA/PVP thin films ($\lambda_{em}^{PVA/PVP}$), emission maximum of TPU thin films (λ_{em}^{TPU}).

Compounds	λ_{em}^{Solid} [nm]	λ_{em}^{PMMA} [nm]	λ_{em}^{SBS} [nm]	$\lambda_{em}^{PVA/PVP}$ [nm]	λ_{em}^{TPU} [nm]
L1	509	472	506	499	493
L2	499	467	471	472	487
L3	469	–	–	–	491

polymer matrix can tune the emission wavelength to better suit the application.

4. Conclusions

In present work, three new bis-dansyl probes containing a sulfide bridge were synthesized and their photophysical properties were studied. Since dansyl compounds are known to exhibit solvatofluorochromism, photophysical studies were carried out in different solvents to fully evaluate the influence of each solvent's intrinsic characteristics on the probes' emission. The equation of Kamlet-Taft was implemented to gain value insights into solute–solvent interactions, and positive solvatofluorochromism behaviour was observed for all compounds. The presence of heteroatoms also enables the study of how metal ions influence the probes' photophysical behaviour. From an environmental remediation perspective, L**1** and **L2** were found to quench their emission in the presence of Hg^{2+} and Cu^{2+} ions. Further calculations suggested that these compounds form mononuclear species with Cu^{2+} and Hg^{2+} and that **L2** has the highest association constant with Hg^{2+} ($LogK_{ass.} = 6.38$) and an LOD and LOQ of 4 μM and 7 μM, respectively. Finally, the probes were characterized in the solid state and doped in solid supports for the development of molecular thermometers PMMA, SBS, PVA/PVP, and TBU doped polymers were synthesized, and their luminescence was studied. The polymer matrix was found to modulate the emission maximum of all compounds and contribute to the emission at higher temperatures than those found in the solid state. Good linearity could also be observed at elevated temperatures, making these probes suitable candidates as temperature sensors in industrial applications.

CRediT authorship contribution statement

Frederico Duarte: Conceptualization, Data curation, Writing – original draft, Writing – review & editing, Visualization, Investigation, Validation, Formal analysis, Methodology. **Georgi Dobrikov:** Conceptualization, Funding acquisition, Data curation, Writing – original draft, Writing – review & editing, Resources. **Atanas Kurutos:** Conceptualization, Funding acquisition, Data curation, Writing – original draft, Writing – review & editing, Resources. **Jose LuisCapelo-Martinez:** Funding acquisition, Writing – original draft, Writing – review & editing, Resources. **Elisabete Oliveira:** Conceptualization, Data curation, Writing – original draft, Writing – review & editing. **Carlos Lodeiro:** Conceptualization, Funding acquisition, Data curation, Writing – original draft, Writing – review & editing, Supervision, Resources.

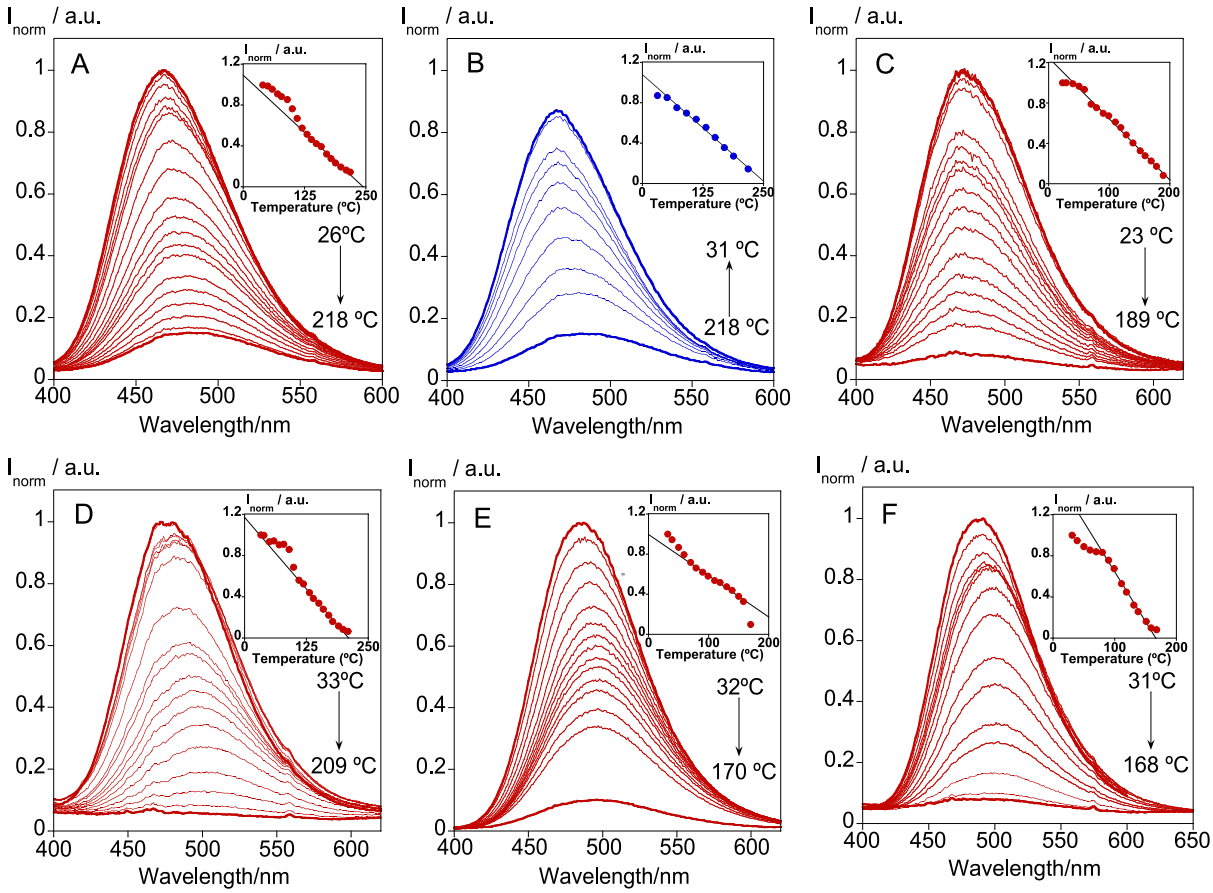

Fig. 8. Temperature-dependent emission spectra of **L2** doped in (A) PMMA during heating cycle [Inset: I_{norm}. vs. T plot at 467 nm upon heating: 120 to 218 °C (Y = 1.0919–0.004465x), yielding R = 0.9948]; (B) PMMA during cooling cycle [Inset: I_{norm}. vs. T plot at 467 nm upon cooling: 51 to 218 °C (Y = 1.0787–0.0042258x), yielding R = 0.99644]; (C) SBS during heating cycle [Inset: I_{norm}. vs. T plot at 471 nm upon heating: 70 to 189 °C (Y = 1.2484–0.0060553x), yielding R = 0.99652]; (D) PVA/PVP during heating cycle [Inset: I_{norm}. vs. T plot at 472 nm upon heating: 110 to 199 °C (Y = 1.1712–0.0055656x), yielding R = 0.99736]; (E) TPU during heating cycle [Inset: I_{norm}. vs. T plot at 487 nm upon heating: 70 to 158 °C (Y = 0.99593–0.00411x), yielding R = 0.99574]. Temperature-dependent emission spectra of **L3** doped in (F) TPU during heating cycle [Inset: I_{norm}. vs. T plot at 491 nm upon heating: 80 to 159 °C (Y = 1.611–0.0096602x), yielding R = 0.99758].

Declaration of Competing Interest

The authors declare that they have no known competing financial interests or personal relationships that could have appeared to influence the work reported in this paper.

Data availability

Data will be made available on request.

Acknowledgements

This work was supported by the Associate Laboratory for Green Chemistry LAQV which is financed by national funds from *Fundação para a Ciência e Tecnologia and Ministério da Ciência, Tecnologia e Ensino Superior* (FCT/MCTES) through the projects UIDB/50006/2020 and UIDP/50006/2020. PROTEOMASS Scientific Society (Portugal) is acknowledged by the funding provided through the General Funding Grant 2022-2023, and by the funding provided to the Laboratory for Biological Mass Spectrometry Isabel Moura (#PM001/2019 and #PM003/2016). F.D. thanks to FCT/MCTES (Portugal) for his doctoral grant 2021.05161.BD. E.O thanks FCT/MCTES (Portugal) for the individual contract, CEECIND/00648/2017. H. M. S. acknowledges the Associate Laboratory for Green Chemistry LAQV (LA/P/0008/2020) funded by FCT/MCTES for his research contract. The financial support by the Bulgarian National Science Fund (BNSF) under grant – "Novel styryl and polymethine fluorophores as potential theranostic agents" contract No KII-06-M59/1 from 15.11.2021 is gratefully acknowledged by A.K. This work is also developed and acknowledged by A.K. as part of contract №: BG-RRP-2.004-0002-C01, Laboratory of Organic Functional Materials (Project BiOrgaMCT), Procedure BG-RRP-2.004 „Establishing of a network of research higher education institutions in Bulgaria", funded by BULGARIAN NATIONAL RECOVERY AND RESILIENCE PLAN".

G. D. thanks to the European Regional Development Fund within the Operational Programme Science and Education for Smart Growth 2014 - 2020 under the Project Center of Excellence: National center of mechatronics and clean technologies - BG05M2OP001-1.001-0008 for the financial support.

Funding

This work received support from PT national funds (FCT/MCTES, *Fundação para a Ciência e Tecnologia* and *Ministério da Ciência, Tecnologia e Ensino Superior*) through the projects UIDB/50006/2020 and UIDP/50006/2020. This work received support from PROTEOMASS Scientific Society through the General Funding Grant 2022-2023, and the projects #PM001/2019 and #PM003/2016.

Appendix A. Supplementary data

Supplementary data to this article can be found online at https://doi.

org/10.1016/j.jphotochem.2023.115033.

References

[1] E.O. Dare, V. Vendrell-Criado, M.C. Jiménez, R. Pérez-Ruiz, D. Díaz Díaz, Highly efficient latent fingerprint detection by eight-dansyl-functionalized octasilsesquioxane nanohybrids, Dyes Pigm. 184 (2021) 108841.

[2] Y. Zhang, B. Lei, X. Zhang, Reversible, controllable white-light emission of dye systems by dynamic covalent furan moiety exchange, Chem. Commun. 58 (2022) 5261–5264, https://doi.org/10.1039/D2CC01309F.

[3] Y. Zhang, B. Lei, X. Zhang, Intramolecular energy transfer dyes as temperature- and polarity-sensitive fluorescence probes, Dye. Pigment. 205 (2022), 110492, https://doi.org/10.1016/j.dyepig.2022.110492.

[4] D. Yang, X.T. Wu, X.J. Cao, B.X. Zhao, A reversible ratiometric fluorescence probe for fast detection of trace water in different organic solvents, Dye. Pigment. 170 (2019), 107558, https://doi.org/10.1016/j.dyepig.2019.107558.

[5] Y. Cui, F. Li, X. Zhang, Controlling fluorescence resonance energy transfer of donor–acceptor dyes by Diels-Alder dynamic covalent bonds, Chem. Commun. 57 (2021) 3275–3278, https://doi.org/10.1039/D1CC00165E.

[6] A.F. Sierra, D. Hernández-Alonso, M.A. Romero, J.A. González-Delgado, U. Pischel, P. Ballester, Optical supramolecular sensing of creatinine, J. Am. Chem. Soc. 142 (2020) 4276–4284, https://doi.org/10.1021/jacs.9b12071.

[7] W.M. Pazin, A.K.A. Almeida, V. Manzoni, J.M.M. Dias, A.C.F. De Abreu, M. Navarro, A.S. Ito, A.S. Ribeiro, I.N. De Oliveira, Thermal and solvatochromic effects on the emission properties of a thienyl-based dansyl derivative, RSC Adv. 10 (2020) 28484–28491, https://doi.org/10.1039/D0RA05949H.

[8] N. Li, W. Qin, Y. Chen, K. Liu, S. Wang, F. Kong, Construction of a robust polarity sensitive platform and its application for tracking of lipid droplets decrease under oxidative stress in live cells, Sensors Actuators B Chem. 346 (2021), 130491, https://doi.org/10.1016/j.snb.2021.130491.

[9] Y. Pan, C. Zhang, S.H. Liu, Y. Tan, J. Yin, Fluorescent switch based on dithienylethene with dansulfonamide in multimedium, Dye. Pigment. 181 (2020), 108546, https://doi.org/10.1016/j.dyepig.2020.108546.

[10] H.J. Lee, M.J. Cho, S.K. Chang, Ratiometric signaling of hypochlorite by the oxidative cleavage of sulfonhydrazide-based rhodamine−Dansyl Dyad, Inorg. Chem. 54 (2015) 8644–8649, https://doi.org/10.1021/acs.inorgchem.5b01284.

[11] W.L. Wu, H.L. Ma, M.F. Huang, J.Y. Miao, B.X. Zhao, Mitochondria-targeted ratiometric fluorescent probe based on FRET for bisulfite, Sensors Actuators, B Chem. 241 (2017) 239–244, https://doi.org/10.1016/j.snb.2016.10.028.

[12] H. Jiang, Z. Li, Y. Kang, L. Ding, S. Qiao, S. Jia, W. Luo, W. Liu, A two-photon fluorescent probe for Cu2+ based on dansyl moiety and its application in bioimaging, Sensors Actuators, B Chem. 242 (2017) 112–117, https://doi.org/10.1016/j.snb.2016.11.033.

[13] B. Uttam, S. Polepalli, S. Sinha, A. Majumder, C.P. Rao, Selective sensing and removal of mercury ions by encapsulating dansyl appended calix[4]conjugate in a zeolitic imidazolate framework as an organic−inorganic hybrid nanomaterial, ACS Appl. Nano Mater. 5 (2022) 11371–11380, https://doi.org/10.1021/acsanm.2c02459.

[14] G. Donadio, R. Di Martino, R. Oliva, L. Petraccone, P. Del Vecchio, B. Di Luccia, E. Ricca, R. Isticato, A. Di Donato, E. Notomista, A new peptide-based fluorescent probe selective for zinc (II) and copper (II), J. Mater. Chem. B 4 (2016) 6979–6988, https://doi.org/10.1039/C6TB00671J.

[15] P. Wang, J. Wu, P. Su, C. Xu, Y. Ge, D. Liu, W. Liu, Y. Tang, Fluorescence "on-off-on" peptide-based chemosensor for selective detection of Cu2+ and S2- and its application in living cells bioimaging, Dalt. Trans. 45 (2016) 16246–16254, https://doi.org/10.1039/C6DT03330J.

[16] A. Aliberti, P. Vaiano, A. Caporale, M. Consales, M. Ruvo, A. Cusano, Fluorescent chemosensors for Hg2+ detection in aqueous environment, Sensors Actuators, B Chem. 247 (2017) 727–735, https://doi.org/10.1016/j.snb.2017.03.026.

[17] X. Pang, J. Dong, L. Gao, L. Wang, S. Yu, J. Kong, L. Li, Dansyl-peptide dual-functional fluorescent chemosensor for Hg2+ and biothiols, Dye. Pigment. 173 (2020), 107888, https://doi.org/10.1016/j.dyepig.2019.107888.

[18] Y. Wang, J. Zhou, L. Zhao, B. Xu, A dual-responsive and highly sensitive fluorescent probe for Cu^{2+} and pH based on a dansyl derivative, Dye. Pigment. 180 (2020), 108513, https://doi.org/10.1016/j.dyepig.2020.108513.

[19] L.J. Ma, J. Liu, L. Deng, M. Zhao, Z. Deng, X. Li, J. Tang, L. Yang, Selective and sensitive fluorescence-shift probes based on two dansyl groups for mercury(II) ion detection *Photochem*, Photobiol. Sci. 13 (2014) 1521–1528, https://doi.org/10.1039/C4PP00094C.

[20] Y.B. Barot, V. Anand, R. Mishra, Di-Triphenylamine-based AIE active Schiff base for highly sensitive and selective fluorescence sensing of Cu^{2+} and Fe^{3+}, J. Photochem. Photobiol. A Chem. 426 (2022), 113785 https://doi.org/10.1016/j.jphotochem.2022.113785.

[21] J. Galhano, G.A. Marcelo, A. Kurutos, E. Bértolo, J.L. Capelo-Martinez, C. Lodeiro, E. Oliveira, Development of low-cost colourimetric and pH sensors based on PMMA@Cyanine polymers, Dye. Pigment. 200 (2022), 110154, https://doi.org/10.1016/j.dyepig.2022.110154.

[22] C. Lodeiro, J.L. Capelo, J.C. Mejuto, E. Oliveira, H.M. Santos, B. Pedras, C. Nuñez, Light and colour as analytical detection tools: A journey into the periodic table using polyamines to bio-inspired systems as chemosensors, Chem. Soc. Rev. 39 (39) (2010) 2948–2976, https://doi.org/10.1039/B819787N.

[23] G.A. Marcelo, S.M.G. Pires, M.A.F. Faustino, M.M.Q. Simões, M.G.P.M.S. Neves, H. M. Santos, J.L. Capelo, J.P. Mota, C. Lodeiro, E. Oliveira, New dual colorimetric/fluorimetric probes for Hg2+ detection & extraction based on mesoporous SBA-16 nanoparticles containing porphyrin or rhodamine chromophores, Dye. Pigment. 161 (2019) 427–437, https://doi.org/10.1016/j.dyepig.2018.09.068.

[24] E. Oliveira, E. Bértolo, C. Núñez, V. Pilla, H.M. Santos, J. Fernández-Lodeiro, A. Fernández-Lodeiro, J. Djafari, J.L. Capelo, C. Lodeiro, Green and red fluorescent dyes for translational applications in imaging and sensing analytes: a dual-color flag, ChemistryOpen 7 (2018) 9–52, https://doi.org/10.1002/open.201700135.

[25] R. Nagarajan, H.-I. Ryoo, B.D. Vanjare, N. Gyu Choi, K.i. Hwan Lee, Novel phenylalanine derivative-based turn-off fluorescent chemosensor for selective Cu2 + detection in physiological pH, J. Photochem. Photobiol. A Chem. 418 (2021) 113435.

[26] T.N. Moshkina, E.V. Nosova, A.E. Kopotilova, M.I. Savchuk, I.L. Nikonov, D. S. Kopchuk, P.A. Slepukhin, G.A. Kim, G.N. Lipunova, V.N. Charushin, Synthesis and photophysical properties of pyridyl- and quinolinyl-substituted 4-(4-aminophenyl)quinazolines, J. Photochem. Photobiol. A Chem. 429 (2022), 113917, https://doi.org/10.1016/j.jphotochem.2022.113917.

[27] S.B. Yadav, S. Kothavale, N. Sekar, Triphenylamine and N-phenyl carbazole-based coumarin derivatives: Synthesis, solvatochromism, acidochromism, linear and nonlinear optical properties, J. Photochem. Photobiol. A Chem. 382 (2019), 111937, https://doi.org/10.1016/j.jphotochem.2019.111937.

[28] H. Sharma, R. Kakkar, S. Bishnoi, M.D. Milton, Synthesis of acceptor-donor-acceptor based phenothiazine-5-oxide aldehydes displaying large Stokes shift- "on-off-on" acidofluorochromic switch and molecular logic gate operation, J. Photochem. Photobiol. A Chem. 430 (2022), 113944, https://doi.org/10.1016/j.jphotochem.2022.113944.

[29] S. Mocanu, G. Ionita, I. Matei, Solvatochromic characteristics of dansyl molecular probes bearing alkyl diamine chains, Spectrochim. Acta A Mol. Biomol. Spectrosc. 237 (2020) 118413.

[30] K. Li, J. Wang, Y. Li, Y. Si, J. He, X. Meng, H. Hou, B.Z. Tang, Combining two different strategies to overcome the aggregation caused quenching effect in the design of ratiometric fluorescence chemodosimeters for pH sensing, Sensors Actuators, B Chem. 274 (2018) 654–661, https://doi.org/10.1016/j.snb.2018.07.109.

[31] S. Areti, S. Bandaru, D.S. Yarramala, C.P. Rao, Optimizing the electron-withdrawing character on benzenesulfonyl moiety attached to a glyco-conjugate to impart sensitive and selective sensing of cyanide in HEPES buffer and on cellulose paper and silica gel strips, Anal. Chem. 87 (2015) 12396–12403, https://doi.org/10.1021/acs.analchem.5b04085.

[32] A. Pucci, Mechanochromic fluorescent polymers with aggregation-induced emission features, Sensors 19 (2019) 4969, https://doi.org/10.3390/s19224969.

[33] B. González-Tobío, F. Duarte, A. Arribas-Delgado, C. Fernández-Lodeiro, J. Fernández-Lodeiro, M. Cano, C. Lodeiro, C. Cuerva, Tuning and reviving the luminescence of a new class of pyridyl β-diketonate Eu(III) metallomesogens: From molecules to entrapment in polymer particles, Dye. Pigment. 204 (2022), 110440, https://doi.org/10.1016/j.dyepig.2022.110440.

[34] R. Jiménez, F. Duarte, S. Nuti, J.A. Campo, C. Lodeiro, M. Cano, C. Cuerva, Thermochromic and acidochromic properties of polymer films doped with pyridyl-β-diketonate boron(III) complexes, Dye. Pigment. 177 (2020), 108272, https://doi.org/10.1016/j.dyepig.2020.108272.

[35] S. Gupta, M.D. Milton, Novel Y-shaped AIEE-TICT active π-extended quinoxalines-based donor–acceptor molecules displaying acidofluorochromism and temperature dependent emission, J. Photochem. Photobiol. A Chem. 424 (2022), 113630, https://doi.org/10.1016/j.jphotochem.2021.113630.

[36] N.M.M. Moura, S. Valentini, V. Cheptene, A. Pucci, M.G.P.M.S. Neves, J.L. Capelo, C. Lodeiro, E. Oliveira, Multifunctional Porphyrin-based dyes for cations detection in solution and thermoresponsive low-cost materials, Dye. Pigment. 185 (2021), 108897, https://doi.org/10.1016/j.dyepig.2020.108897.

[37] C. Papucci, A. Dessì, C. Coppola, A. Sinicropi, G. Santi, M. Di Donato, M. Taddei, P. Foggi, L. Zani, G. Reginato, A. Pucci, M. Calamante, A. Mordini, Benzo[1,2-d:4,5-d′]bisthiazole fluorophores for luminescent solar concentrators: synthesis, optical properties and effect of the polymer matrix on the device performances, Dye. Pigment. 188 (2021), 109207, https://doi.org/10.1016/j.dyepig.2021.109207.

[38] C. Micheletti, V.A. Dini, M. Carlotti, F. Fuso, D. Genovese, N. Zaccheroni, C. Gualandi, A. Pucci, Blending or Bonding? Mechanochromism of an Aggregachromic Mechanophore in a Thermoplastic Elastomer, ACS Appl. Polym. Mater. 5 (2023) 1545–1555, https://doi.org/10.1021/acsapm.2c02037.

[39] G.A. Marcelo, J. Galhano, M.P. Duarte, A. Kurutos, J.L. Capelo-Martínez, C. Lodeiro, E. Oliveira, Functional cyanine-based PVA:PVP polymers as antimicrobial tools toward food and health-care bacterial infections, Macromol. Biosci. 22 (2022) 1–12, https://doi.org/10.1002/mabi.202200244.

[40] L.M. Porosa, K.B. Mistry, A. Mocella, H. Deng, S. Hamzehi, A. Caschera, A.J. Lough, G. Wolfaardt, D.A. Foucher, Synthesis, structures and properties of self-assembling quaternary ammonium dansyl fluorescent tags for porous and non-porous surfaces, J. Mater. Chem. B 2 (2014) 1509–1520, https://doi.org/10.1039/C3TB21633K.

[41] Y.Y. Xiao, X.L. Gong, Y. Kang, Z.C. Jiang, S. Zhang, B.J. Li, Light-, pH- and thermal-responsive hydrogel with triple-shape memory effect, Chem. Commun. 52 (2016) 10609–10612, https://doi.org/10.1039/C6CC03587F.

[42] H. Yu, B. Zhao, J. Guo, K. Pan, J. Deng, Stimuli-responsive circularly polarized luminescent films with tunable emission, J. Mater. Chem. C 8 (2020) 1459–1465, https://doi.org/10.1039/C9TC06105C.

[43] F. Duarte, G. Dobrikov, A. Kurutos, H.M. Santos, J. Fernández-Lodeiro, J.L. Capelo-Martinez, E. Oliveira, C. Lodeiro, Enhancing water sensing via aggregation-induced emission (AIE) and solvatofluorochromic studies using two new dansyl derivatives containing a disulfide bound: Pollutant metal ions detection and preparation of water-soluble fluorescent polymeric particles, Dye. Pigment. 218 (2023), 111428, https://doi.org/10.1016/j.dyepig.2023.111428.

[44] M. Carcelli, D. Rogolino, A. Bacchi, G. Rispoli, E. Fisicaro, C. Compari, M. Sechi, A. Stevaert, L. Naesens, Metal-chelating 2–hydroxyphenyl amide pharmacophore for inhibition of influenza virus endonuclease, Mol. Pharm. 11 (2014) 304–316, https://doi.org/10.1021/mp400482a.

[45] H.L. Yu, W.Y. Wang, B. Hong, Y. Zong, Y.L. Si, Z.Q. Hu, Variational first hyperpolarizabilities of 2,3-naphtho-15-crown-5 ether derivatives with cation-complexing: a potential and selective cation detector, Phys. Chem. Chem. Phys. 18 (2016) 26487–26494, https://doi.org/10.1039/C6CP04577D.

[46] A. Nion, P. Jiang, A. Popoff, D. Fichou, Rectangular nanostructuring of Au(III) surfaces by self-assembly of size-selected thiacrown ether macrocycles, J. Am. Chem. Soc. 129 (2007) 2450–2451, https://doi.org/10.1021/ja068709e.

[47] M. Montalti, A. Credi, L. Prodi, M.T. Gandolfi, Handbook of Photochemistry, 3rd ed., Taylor & Francis, Boca Raton, BOCA, 2006.

[48] D. MacDougall, W.B. Crummett, et al., Guidelines for data acquisition and data quality evaluation in environmental chemistry, Anal. Chem. 52 (14) (1980) 2242–2249.

[49] G.L. Long, J.D. Winefordner, Limit of detection A closer look at the IUPAC definition, Anal. Chem. 55 (1983) 713A–A724, https://doi.org/10.1021/ac00258a724.

[50] E. Oliveira, R.M.F. Baptista, S.P.G. Costa, M.M.M. Raposo, C. Lodeiro, Solvatochromic effects of bis(indolyl)thienylaril derivatives as new colored materials, Photochem. Photobiol. Sci. 13 (2014) 492–498, https://doi.org/10.1039/C3PP50352F.

[51] P. Gans, A. Sabatini, A. Vacca, Investigation of equilibria in solution. Determination of equilibrium constants with the HYPERQUAD suite of programs, *Talanta* 43 (1996) 1739–1753, https://doi.org/10.1016/0039-9140(96)01958-3.